CrossMark

Thermoelectric Performance of *n*-Type Bi_2Te_3/Cu Composites Fabricated by Nanoparticle Decoration and Spark Plasma Sintering

F.R. SIE,[1,2] C.H. KUO,[1,3] C.S. HWANG,[1,4] Y.W. CHOU,[2] C.H. YEH,[2]
Y.L. LIN,[2] and J.Y. HUANG[3]

1.—Department of Materials Science and Engineering, National Cheng Kung University, Tainan 701, Taiwan. 2.—Green Energy & Environment Laboratories, Industrial Technology Research Institute, Hsinchu 310, Taiwan. 3.—New Materials Research & Development Department, China Steel Company, Kaohsiung 812, Taiwan. 4.—e-mail: cshwang@mail.ncku.edu.tw

Dense *n*-type Bi_2Te_3/Cu composites were prepared using Cu-based acetate decomposition and spark plasma sintering at 673 K and 50 MPa. The effects of Cu addition into ball-milled Bi_2Te_3 on the thermoelectric properties of composites were investigated. The scanning electron microscopy results reveal that Cu nanoparticles with a size of 50–100 nm were dispersed in the Bi_2Te_3 matrix and also pinned at Bi_2Te_3 grain boundaries. The thermoelectric performance of all specimens was measured in the temperature range of 300–500 K. The electrical conduction transformed from metallic to semiconducting with an increase in Cu content due to a decrease in carrier concentration. Hence, the variation in the carrier concentration is determined by the role of Cu dopant in Bi_2Te_3. Furthermore, the thermal conductivity decreased due to lower electronic thermal conductivity and electrical conductivity. In comparison with Bi_2Te_3, the room-temperature *ZT* value for the Bi_2Te_3/Cu (1.0 wt.%) sample increased from 0.31 to 0.60 due primarily to the significant increase in the power factor and reduction in thermal conductivity.

Key words: *n*-Type Bi_2Te_3/Cu composites, spark plasma sintering, carrier concentration, electrical conductivity

INTRODUCTION

Bismuth telluride (Bi_2Te_3)-based compounds are the main thermoelectric materials within the temperature range of 300–500 K. Bi_2Te_3 compounds have an obvious anisotropic crystal structure and belong to the rhombohedral structure, which constitutes five layers, in the order of Te (1)-Bi-Te (2)-Bi-Te (1), along the c-axis. However, this anisotropic structure has poor mechanical properties because of a weak van der Waals force between Te (1)-Te (1) layers.[1,2] Zhao et al.[3] and Kuo et al.[4] reported that anti-site defects in the Bi_2Te_3 system were observed after high energy ball milling, which donated excess electrons. In addition, the Te (1)-Te (1) layers

provide a good diffusion path for external atoms.[5] Han et al.[6] reported that the electrical transport behavior changed from *p*- to *n*-type when Cu content was increased. In their experiments, Cu atoms were located at intercalation sites and played the role of a donor in the melting process. The highest *ZT* value (1.15) was obtained for the $Cu_{0.07}Bi_2Te_3$ specimen. Lee et al.[7] reported a similar effect and obtained an optimized *ZT* of 0.73 for *n*-type Cu-intercalated $Bi_2Te_{2.7}Se_{0.3}$. Liu et al.[8] found that Cu-doped $Bi_2Te_{2.7}Se_{0.3}$ had an optimized *ZT* value of 0.99. When the texture of the Cu-doped $Bi_2Te_{2.7}Se_{0.3}$ sample was changed by re-pressing, the *ZT* value increased from 0.99 to 1.06 in their experiments. However, a different phenomenon has been reported that Cu atoms can substitute into Bi sites, which exhibited a *p*-type conduction behavior of Cu in Bi_2Te_3 system.[9–11] Yu et al.[10] indicated that the

substitution of Bi with Cu led to decreases in the carrier concentration and electrical conductivity and increases in the Seebeck coefficient and power factor. Chen et al.[11] recently used the density of state (DOS) calculation to explain the location of Cu atoms in Bi_2Te_3. According to their reports, the substitution of Cu for Bi is easier than the intercalation of Cu into the van der Waals layer, which means that Cu can act as both a donor and an acceptor in Bi_2Te_3.

Many studies prepared Cu-doped Bi_2Te_3 alloys via a melting process, which led to Cu being located at the intercalation sites between Te (1)-Te (1). Because the solubility of Cu in Bi_2Te_3 is low during melting, it is difficult to observe Cu at Bi sites. In order to determine the location of Cu in Bi_2Te_3, in this study, Cu particles were dispersed on milled Bi_2Te_3 powders and then rapidly compacted by SPS at 673 K and 50 MPa. The thermoelectric transport properties of Bi_2Te_3/Cu bulk samples were investigated.

EXPERIMENTAL PROCEDURES

Commercial Bi_2Te_3 (99.98%, Alfa Aesar) powder, used as the raw material, was subjected to attritor ball milling (01-HD, Union Process) at 600 rpm for 6 h under an argon atmosphere using a stainless steel jar and balls with a diameter of 3 mm. The milled Bi_2Te_3 powders were dry-mixed with copper acetate $((CH_3COO)_2Cu, Cu(OAc)_2)$ powders for 1 h. The mixed powders of milled Bi_2Te_3 and copper acetate were heated at 573 K for 3 h under an argon atmosphere, which led to the decomposition of $Cu(OAc)_2$ to Cu, which bonded to the surface of the milled Bi_2Te_3 powders. Subsequently, Bi_2Te_3 and Bi_2Te_3/Cu powders were sintered under a uniaxial pressure of 50 MPa at 673 K for 5 min in an argon atmosphere using SPS (Dr. Sinter, SPS-systex).

The crystal phases of bulk samples were confirmed by x-ray diffraction (XRD, D8 DISCOVER, Bruker) at room temperature using CuKα radiation (λ = 0.15406 nm). Field-emission scanning electron microscopy (JEOL, FE-SEM 7000F, Japan), energy-dispersive x-ray spectroscopy (EDS), and inductively coupled plasma mass spectrometry (ICP-MS, PerkinElmer, USA) were used to observe the microstructure and composition of sintered samples. The bulk samples were cut into rectangular bars (3 mm × 3 mm × 15 mm) for the measurement of electrical conductivity and Seebeck coefficient under a low inert-gas atmosphere at temperatures ranging from 300 K to 500 K using commercial equipment (ULVAC-RIKO, ZEM-3, Japan). The carrier concentration and mobility of bulk samples were measured using four-probe Hall-effect measurements at room temperature. The thermal diffusivity (α), bulk density (ρ), and specific heat (C_p) were measured using a laser flash thermal constant analyzer (NETZSCH, LFA447, Germany), the Archimedes method, and

differential scanning calorimetry (SETARAM, SENSYS EVO DSC, France), respectively. The thermal conductivity (κ) was calculated using the equation $\kappa = \alpha\rho C_p$.

RESULTS AND DISCUSSION

Figure 1 presents the XRD patterns and lattice parameters of Bi_2Te_3/Cu bulk samples with 0–1.0 wt.% Cu prepared via thermal decomposition and SPS at 673 K. All the diffraction peaks coincide with the rhombohedral structure of Bi_2Te_3 (PDF#15-0863), and no other crystalline phases are formed. The orientation factor F was calculated using the following equations:[12]

$$F = \frac{P - P_0}{1 - P_0} \qquad (1)$$

$$P_0 = \frac{I_0(00l)}{\sum I_0(hkl)} \qquad (2)$$

$$P = \frac{I(00l)}{\sum I(hkl)} \qquad (3)$$

where P and P_0 are the integrated intensities of all $(00l)$ planes to the intensities of all (hkl) planes for preferentially and randomly oriented samples, respectively. The orientation factor F ranged from 0.02 to 0.05, which is lower than previously reported values.[13,14] This may indicate that there is no preferential orientation in the present samples. The a- and c-axis lattice parameters for the Bi_2Te_3 bulk sample without Cu addition were 4.381 Å and 30.493 Å, respectively. When Cu was embedded into the Bi_2Te_3 matrix, these lattice parameters increased to 4.386 and 30.543 Å, respectively. These results reveal that Cu^+ ions diffused into Bi_2Te_3 and changed the c-axis lattice parameters. Many studies have demonstrated that Cu atoms diffuse rapidly and locate at the intercalation sites of the Te (1)-Te (1) layer, which increases the c-axis lattice parameters and donates free electrons, in $Cu_xBi_2Te_3$[6] and $Cu_xBi_2Te_{2.7}Se_{0.3}$.[7,8] The actual Cu content and the Bi/Te ratio in SPS samples were determined using ICP-MS and EDS, as shown in Table I. The results confirm the incorporation of Cu into Bi_2Te_3 and show good consistency when the nominal Cu content was increased. Moreover, even though all samples were Te-poor, their Bi/Te ratio remained almost constant.

Figure 2 shows SEM images of the fractured surface for all dense bulk samples obtained by SPS. All bulk samples show a dense morphology (Fig. 2a–d). The fractured surface of the Bi_2Te_3 specimen had a clean grain surface (Fig. 2e). For the Bi_2Te_3/Cu specimens (Fig. 2f–h), Cu nanoparticles (50–100 nm) were confirmed from EDS. They were well dispersed in the Bi_2Te_3 matrix and pinned at Bi_2Te_3 grain boundaries. When the number of Cu nanoparticles increased, the grain size of all

Thermoelectric Performance of n-Type Bi_2Te_3/Cu Composites Fabricated by Nanoparticle Decoration and Spark Plasma Sintering

1929

samples did not significant change, remaining in the range of 1–3 μm.

The carrier concentration and mobility values of Bi_2Te_3 and Bi_2Te_3/Cu samples from Hall-effect measurements are also listed in Table I. The carrier concentration values of all specimen are negative, indicating that electrons are the main contributors of electric transport charge. When increasing Cu content from 0 wt.% to 1.0 wt.%, the carrier con-

Fig. 1. (a) XRD patterns of sample sections perpendicular and parallel to pressing direction and (b) lattice parameters of Bi_2Te_3 and Bi_2Te_3/Cu bulk samples with various Cu content level prepared by thermal decomposition and SPS at 673 K.

centration initially decreased from 7.98×10^{19} cm^{-3} to 1.17×10^{19} cm^{-3}, and the slightly increased to 1.30×10^{19} cm^{-3}, whereas the carrier mobility increased from 121 cm^2/Vs to 241 cm^2/Vs at room temperature. Generally, the carrier concentration increases when Cu atoms are located at the intercalation sites of the van der Waals layer as a donor.[6,15] However, there is a different trend for carrier concentration, which initially decreased and then slightly increased in this experiment. This means that there are different carrier types in the Bi_2Te_3/Cu system. According to the lattice parameters and Hall-effect measurements, the reduction of carrier concentration may decrease the intrinsic defects of $Te_{Bi}^{\cdot}$ anti-site defects in Bi_2Te_3 when Cu atoms are located at the intercalation sites of Te (1)-Te (1). However, at high Cu concentration (1.0 wt.%), the influence of Cu atoms at intercalation sites as donors overcomes the decrease in the intrinsic defects of $Te_{Bi}^{\cdot}$ anti-site defects, and thus slightly increases the carrier concentration. Furthermore, Cu nanoparticles could not efficiently donate electrons, but provided an extra interface to scatter carriers. Hence, the effect of carrier concentration is determined by the Cu atoms that diffuse from Cu nanoparticles to Bi_2Te_3. Although the Bi_2Te_3/Cu system shows two opposite carrier transport types, the main electric transport charge is still electrons. The carrier mobility increased because the intrinsic defects of $Te_{Bi}^{\cdot}$ in Bi_2Te_3 and the total carrier concentration decreased. However, for the Bi_2Te_3/Cu (1.0 wt.%) specimen, the carrier mobility still increased though the carrier concentration increased only slightly. An increase in carrier concentration typically leads to a decrease in carrier mobility due to an enhancement of the carrier scattering effect. Svechnikova,[16] Wang,[15] and Liu[8] observed that Cu entered the intercalation sites between van der Waals layers, increasing both carrier concentration and mobility, which was probably the bridging effect to mitigate the interface scattering. Figure 3 shows the mobility as a function of carrier concentration, and it is obvious that mobility shows an approximate $n^{-0.34}$ relation for the Bi_2Te_3/Cu system. Accordingly, it reveals a rough consistency and indicates that Cu has no significant influence on the electron
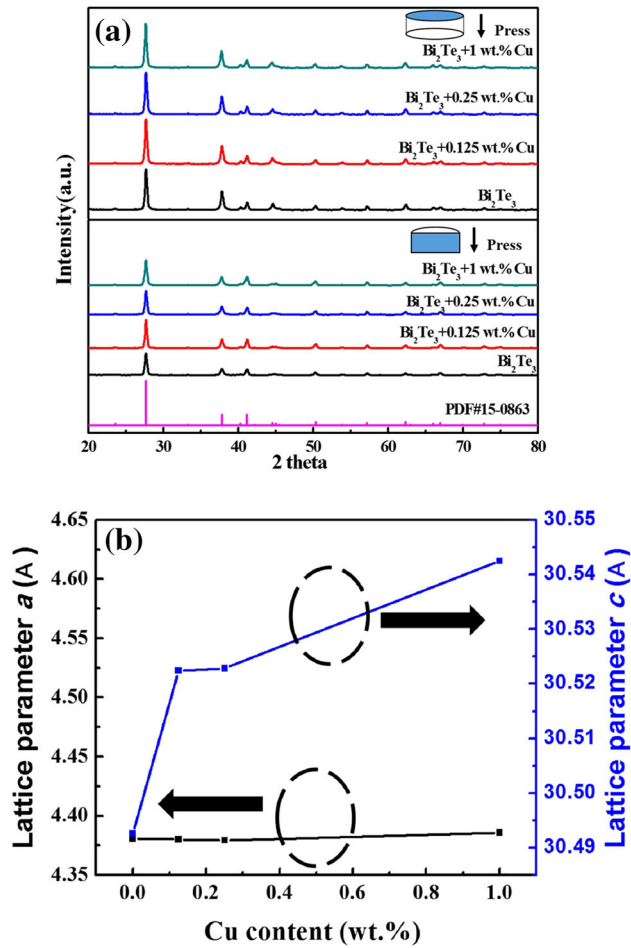
Table I. Actual Cu content (ICP-MS), Bi/Te ratio (EDS), carrier concentration, and mobility for Bi_2Te_3 and Bi_2Te_3/Cu bulk samples measured at room temperature

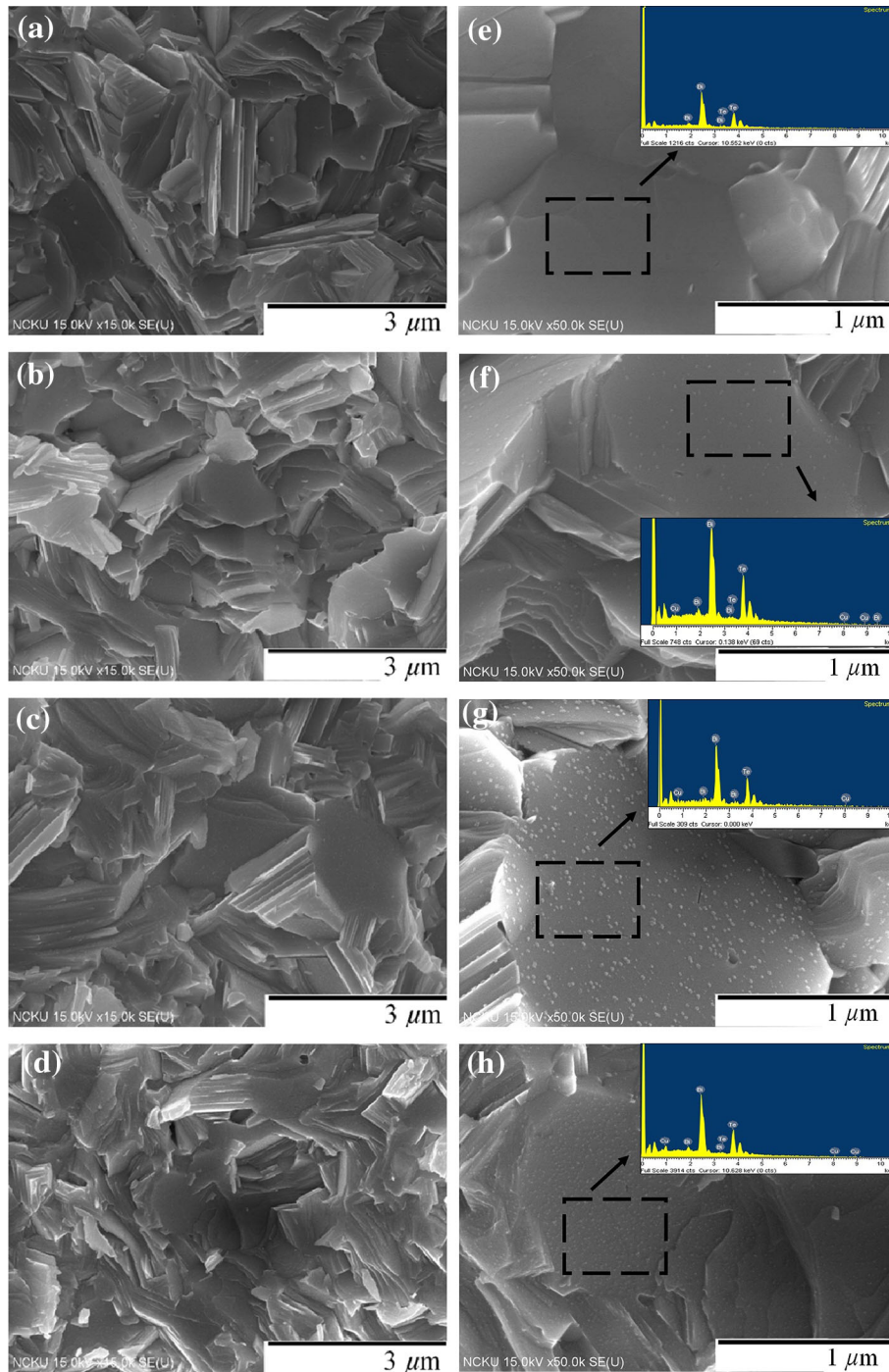| Sample	Actual Cu content (wt.%)	Bi/Te ratio	Type (p/n)	Carrier concentration (cm^{-3})	Mobility (cm^2/Vs)
BT	0	2/2.97	n	7.98×10^{19}	121
BT + 0.125 wt.% Cu	0.119	2/2.99	n	2.94×10^{19}	172
BT + 0.25 wt.% Cu	0.223	2/2.98	n	1.17×10^{19}	217
BT + 1.0 wt.% Cu	0.865	2/2.99	n	1.30×10^{19}	241

Fig. 2. SEM images of fractured surface at ×15,000 magnification of (a) Bi_2Te_3, (b) Bi_2Te_3/0.125 wt.% Cu, (c) Bi_2Te_3/0.25 wt.% Cu, and (d) Bi_2Te_3/1.0 wt.% Cu. Corresponding images at 50,000x magnification and EDS spectra shown in (e), (f), (g), and (h), respectively. Samples were prepared by thermal decomposition and SPS at 673 K.

scattering mechanism and thus acoustic phonon scattering is dominant.

The temperature dependence of the electrical conductivity for all sintered samples is shown in Fig. 4. The electrical conductivity decreased from 1544 S/cm to 407 S/cm and then increased to 501 S/cm at room temperature when the Cu concentration was increased from 0 wt.% to 1.0 wt.%. In addition,

a conversion between metallic and semiconducting states was observed at different Cu concentrations within the measured temperature range. The electrical conductivity decreased with increasing measured temperature for the Bi_2Te_3 sample, exhibiting a metallic (degenerate semiconductor) characteristic. In contrast, the electrical conductivity shows semiconductor behavior for all Bi_2Te_3/Cu samples,
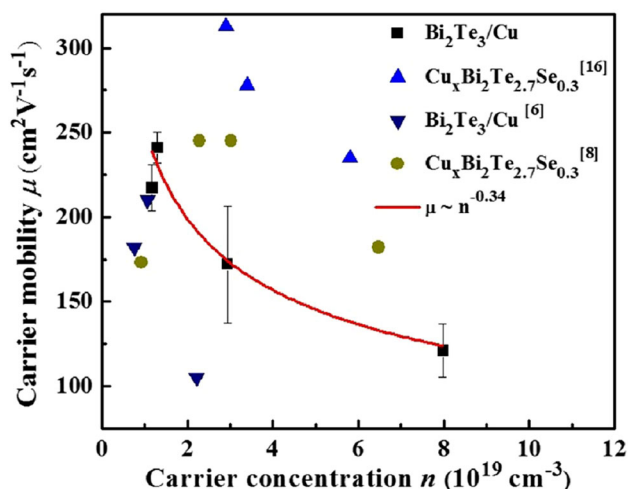
Thermoelectric Performance of *n*-Type Bi₂Te₃/Cu Composites Fabricated by Nanoparticle Decoration and Spark Plasma Sintering

1931

Fig. 3. The carrier mobility as a function of carrier concentration for Bi₂Te₃/Cu samples with 0–1.0 wt.% Cu. Solid line represents the $\mu \sim n^{-0.34}$ relation.
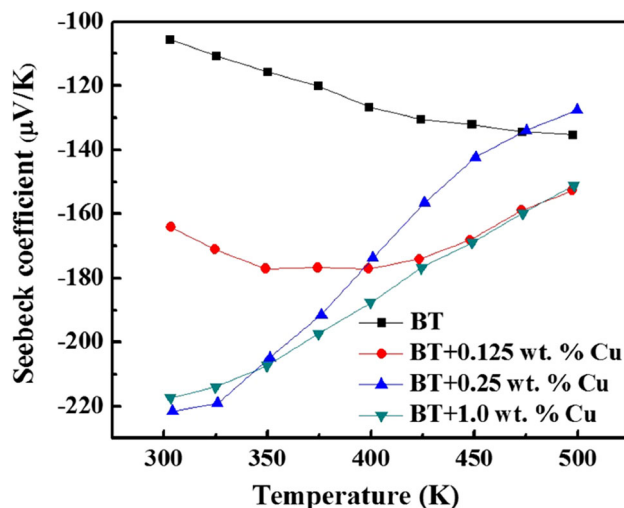

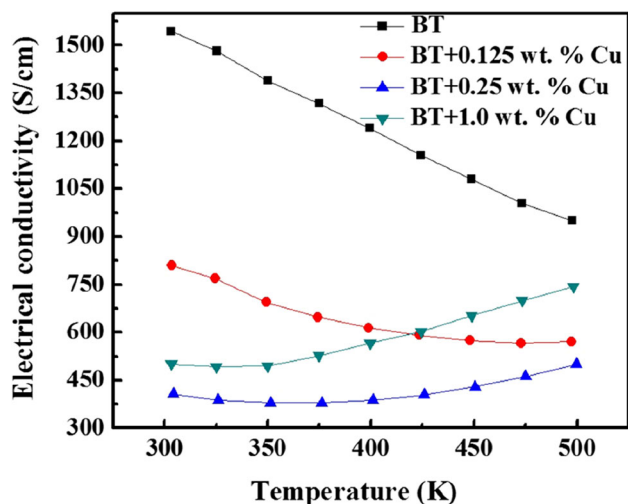Fig. 5. Temperature dependence of Seebeck coefficient for Bi₂Te₃/Cu samples with 0–1.0 wt.% Cu.

Fig. 4. Temperature dependence of electrical conductivity for Bi₂Te₃/Cu samples with 0–1.0 wt.% Cu.
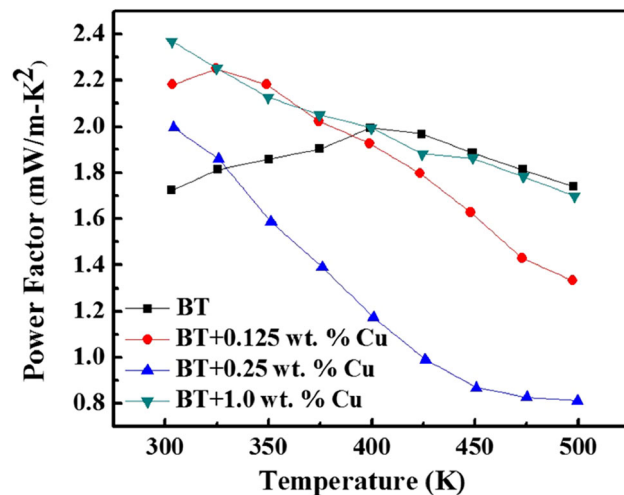

Fig. 6. Temperature dependence of power factor for Bi₂Te₃/Cu samples with 0–1.0 wt.% Cu.

which increases with higher measured temperature. Normally, Bi₂Te₃ is a narrow band-gap semiconductor and exhibits a bipolar effect, in which the thermal excitation of carriers from the valence band to the conduction band generates holes and electrons.[17,18] Because Bi₂Te₃ generates a greater number of electrons after mechanical treatment, the position of the Fermi level is inside the conduction band at low temperature and a degenerate semiconductor (metallic) characteristic is found (the bipolar effect is inhibited at elevated temperature). When the Cu concentration is increased, more Cu⁺ ions occupy the intercalation sites of the van der Waals layers of Bi₂Te₃ and the intrinsic defects of $Te^{\cdot}_{Bi}$ in Bi₂Te₃ is eliminated, which decreases the carrier concentration and electrical conductivity. In addition, the bonding between Cu nanoparticles and

Bi₂Te₃ is a possible reason for the Fermi level decreasing to the valence band. Hence, the movement of the Fermi level and the decrease in carrier concentration change the electronic transport properties from metallic to semiconducting when Cu is embedded in Bi₂Te₃. However, for the Bi₂Te₃/Cu (1.0 wt.%) specimen, despite the fact that an enhancement of carrier concentration results in an upward shift to the conduction band, the electrical conductivity exhibits semiconducting behavior. On the other hand, the bipolar effect was clearly observed for all Bi₂Te₃/Cu samples, exhibiting a decrease and then an increase in electrical conductivity. According to Fig. 4, an obvious turn-over temperature of electrical conductivity for the Bi₂Te₃/Cu (0.25 and 1.0 wt.%) specimens are 350 K and 325 K, respectively. Because the Bi₂Te₃/

Cu (1.0 wt.%) has a greater carrier concentration and closer conduction band, its turn-over temperature of electrical conductivity decreases.

Figure 5 shows the temperature dependence of the Seebeck coefficient for all bulk samples measured from 300 K to 500 K. All samples have a negative Seebeck coefficient, so the electrical conduction behavior is contributed mainly by electrons. The absolute values of the Seebeck coefficient for Bi_2Te_3 and Bi_2Te_3/Cu increased significantly from 106 μV/K to 221 μV/K and then decreased slightly to 217 μV/K at room temperature. Furthermore, the opposite tendency of the Seebeck coefficient was observed in the measured temperature range of 300–500 K. When the measured temperature was increased, the Seebeck coefficient increased for Bi_2Te_3 , but decreased for all Bi_2Te_3/Cu samples. When Cu nanoparticles were added into Bi_2Te_3 matrix and sintered rapidly, the total carrier concentration of Bi_2Te_3/Cu decreased, and thus the Seebeck coefficient of the Bi_2Te_3/Cu increased at room temperature. Additionally, the Seebeck coefficient for the Bi_2Te_3 sample increased with temperature due to the metallic (degenerate semiconductor) behavior. The relatively low total carrier concentrations are obtained for Bi_2Te_3/Cu (0.25 and 1.0 wt.%) samples, the Fermi level is shifted, which leads to semiconducting behavior.
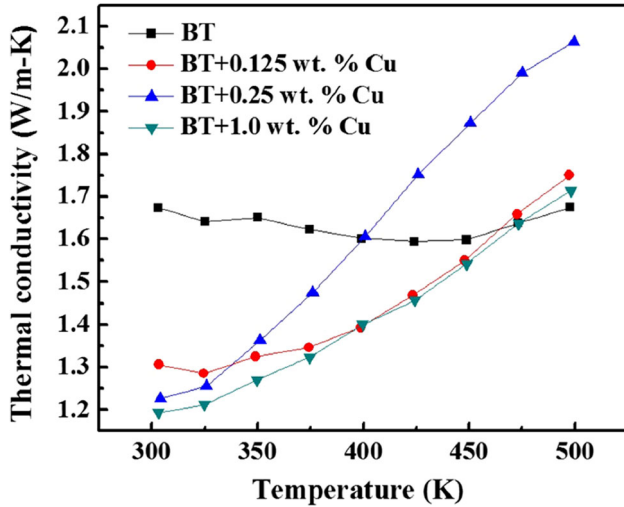
For non-degenerate semiconductors, the thermal excitation of intrinsic carriers leads to an increase in the carrier concentration and a decrease in the Seebeck coefficient with increasing measured temperature.

Figure 6 shows the temperature dependence of the power factor ($S^2\sigma$) for all bulk samples. The values of the power factor for Bi_2Te_3/Cu samples are larger than those of Bi_2Te_3 at room temperature. The power factor increased from 1.72 mW/m K^2 to 2.37 mW/m K^2 at room temperature with increasing Cu content. The enhancement of the power factor is due to the appropriate electrical conductivity and Seebeck coefficient. Based on the results, the carrier transport properties are adjusted through the Cu concentration and position of Cu^+ in Bi_2Te_3.

Figure 7 shows the temperature dependence of thermal conductivity for all sintered samples. The thermal conductivity decreased from 1.67 W/m K to 1.19 W/m K at room temperature with increasing Cu content. All Bi_2Te_3/Cu specimens demonstrate obvious bipolar conduction since the thermal conductivity rapidly increased with measured temperature, which is consistent with the electrical conductivity results. The total thermal conductivity (κ) is the sum of the electronic thermal conductivity (κ_e) and the phonon thermal conductivity (κ_l), and calculated using the following equation: $\kappa = \kappa_l + \kappa_e = \kappa_l + L\sigma T$. The electronic thermal conductivity (κ_e) can be estimated using the Wiedemann-Frantz equation ($\kappa_e = L\sigma T$), where L is the Lorentz number. The Lorentz number depends on the scattering parameter γ and the reduced Fermi energy η. The equation for L can be given as[19]:

$$L = \left(\frac{\kappa_B}{e}\right)^2 \left(\frac{(\gamma+7/2)F_{\gamma+5/2}(\eta)}{(\gamma+3/2)F_{\gamma+1/2}(\eta)} - \left[\frac{(\gamma+5/2)F_{\gamma+3/2}(\eta)}{(\gamma+3/2)F_{\gamma+1/2}(\eta)}\right]^2\right)$$

(4)

Based on this equation, the calculation of Fermi energy η is necessary. It can be derived from the Seebeck coefficient using the following relationship:[19,20]

$$S = \pm \frac{\kappa_B}{e}\left(\frac{(\gamma+5/2)F_{\gamma+3/2}(\eta)}{(\gamma+3/2)F_{\gamma+1/2}(\eta)} - \eta\right)$$

(5)

where $F_n(\eta)$ is the Fermi integral, which can be expressed as follows:[19,20]

Fig. 7. Temperature dependence of thermal conductivity for Bi_2Te_3/Cu samples with 0–1.0 wt.% Cu.

Table II. κ_{total}, κ_e, κ_l, and Lorenz constant L for Bi_2Te_3 and Bi_2Te_3/Cu bulk samples measured at room temperature

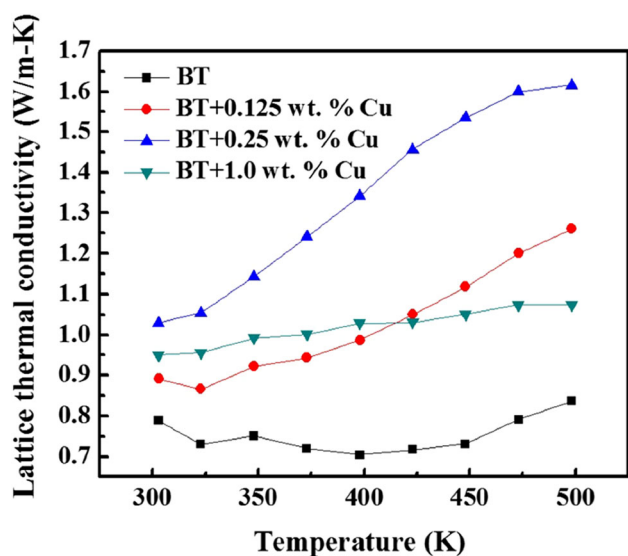| Sample	κ_{total} (W/m K)	κ_e (W/m K)	κ_l (W/m K)	L (10^{-8} V^2 K^{-2})
BT	1.67	0.88	0.79	1.9
BT + 0.125 wt.% Cu	1.31	0.41	0.89	1.7
BT + 0.25 wt.% Cu	1.23	0.20	1.03	1.6
BT + 1.0 wt.% Cu	1.19	0.24	0.95	1.6

Thermoelectric Performance of *n*-Type Bi$_2$Te$_3$/Cu Composites Fabricated by Nanoparticle Decoration and Spark Plasma Sintering

1933

Fig. 8. Temperature dependence of lattice thermal conductivity for Bi$_2$Te$_3$/Cu samples with 0–1.0 wt.% Cu.
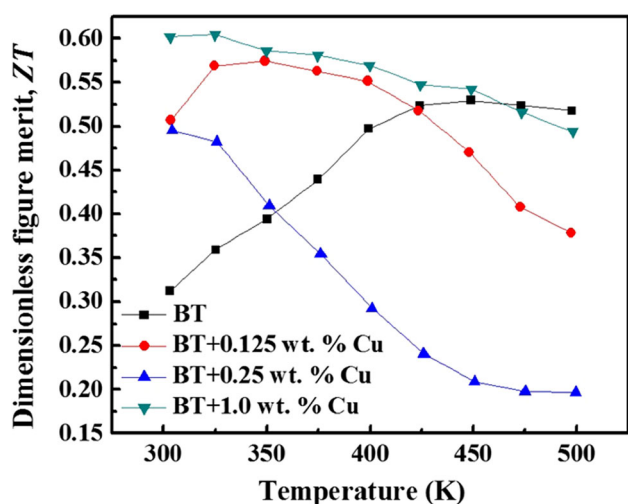

Fig. 9. Temperature dependence of dimensionless *ZT* values for Bi$_2$Te$_3$/Cu samples with 0–1.0 wt.% Cu.

$$F_n(\eta) = \int_0^\infty \frac{\chi^n}{1 + e^{\chi - \eta}} d\chi \qquad (6)$$

In the above equations, κ_B and e are the Boltzmann's constant and the electronic charge of the carriers, respectively. According to the results of Fig. 3, the main scattering mechanism is the acoustic phonon scattering, and the γ value is $-1/2$. Therefore, the Lorenz number can be obtained from the above equations, as seen in Table II. Moreover, the lattice thermal conductivity values were obtained according to $\kappa - \kappa_e$, with the results shown in Fig. 8. The decrease in electronic thermal conductivity is the main reason for the reduction in the total thermal conductivity. Generally, a decrease of

lattice thermal conductivity is facilitated by nanostructures, which provide extra phonon scattering. When Cu reacted with Bi$_2$Te$_3$, the electronic thermal conductivity decreased significantly because of the reduced electrical conductivity. Additionally, a decrease in the intrinsic defects of Te$_{Bi}^{\cdot}$ anti-site defects lead to a reduction in carrier concentration, and thus may have increased the lattice thermal conductivity of Bi$_2$Te$_3$. Although nanoparticles[21–24] and nanostructure[25,26] have been found to act as scattering phonons in many studies, this could not be clearly observed in the present work. According to the results shown in Figs. 7 and 8, defects in the Bi$_2$Te$_3$/Cu system play a key role in the reduction of thermal conductivity.

Figure 9 presents the temperature dependence of *ZT* value for all samples. The room-temperature *ZT* values for all Bi$_2$Te$_3$/Cu samples are greater than that of Bi$_2$Te$_3$. The maximum *ZT* value of the Bi$_2$Te$_3$/Cu (1.0 wt.%) sample is about 0.6 at room temperature, and the *ZT* value notably increased within a wide temperature range from 300 K to 450 K. In comparison with Bi$_2$Te$_3$, the *ZT* value for the Bi$_2$Te$_3$/Cu (1.0 wt.%) sample increased from 0.31 to 0.60 due primarily to the significant increase in the power factor and reduction in thermal conductivity.

CONCLUSION

Bi$_2$Te$_3$/Cu thermoelectric composites have been successfully synthesized by Cu based acetate decomposition and SPS. Dense *n*-type Bi$_2$Te$_3$/Cu composites were obtained, and Cu nanoparticles are well dispersed in all Bi$_2$Te$_3$/Cu bulk samples. Additionally, the interaction of Cu$^+$ ions at intercalation sites and intrinsic defects of Te$_{Bi}^{\cdot}$ changed carrier transport behavior. The results show that Cu$^+$ ions occupied the intercalation sites of Te (1)-Te (1) as a donor, which led to a variation in carrier concentration and a movement of the Fermi level. Hence, the electrical conductivity changed from metallic to semiconducting states when the Cu content was increased. The *ZT* value of the Bi$_2$Te$_3$/Cu system increased owing to a higher power factor and lower thermal conductivity at room temperature, which were controlled by the concentration of Cu nanoparticles. In comparison with Bi$_2$Te$_3$, the maximum *ZT* value of Bi$_2$Te$_3$/Cu (1.0 wt.%) increased from 0.31 to 0.60 at room temperature.

REFERENCES

1. D.M. Rowe, *Thermoelectrics Handbook: Micro to Nano* (New York: CRC Press, 2006), p. 211.
2. L.D. Zhao, B.P. Zhang, J.F. Li, M. Zhou, and W.S. Liu, *Phys. B* 400, 11 (2007).

3. L.D. Zhao, B.P. Zhang, W.S. Liu, H.L. Zhang, and J.F. Li, *J. Alloys Compd.* 467, 91 (2009).
4. C.H. Kuo, C.S. Hwang, M.S. Jeng, W.S. Su, Y.W. Chou, and J.R. Ku, *J. Alloys Compd.* 496, 687 (2010).
5. F.K. Aleskerov and S.Sh. Kakhramanov, *Inorg. Mater.* 45, 975 (2009).
6. M.K. Han, K. Ahn, H. Kim, J.S. Rhyee, and S.J. Kim, *J. Mater. Chem.* 21, 11365 (2011).
7. K.H. Lee, S.M. Choi, S.I. Kim, J.W. Roh, D.J. Yang, W.H. Shin, H.J. Park, K. Lee, S. Hwang, J.H. Lee, H. Mun, and S.W. Kim, *Curr. Appl. Phys.* 15, 190 (2015).
8. W.S. Liu, Q. Zhang, Y. Lan, S. Chen, X. Yan, Q. Zhang, H. Wang, D. Wang, G. Chen, and Z. Ren, *Adv. Energy Mater.* 1, 577 (2011).
9. J.L. Cui, L.D. Mao, W. Yang, X.B. Wu, D.Y. Chen, and W.J. Xiu, *J. Solid State Chem.* 180, 3583 (2007).
10. H.J. Yu, M. Jeong, Y.S. Lim, W.S. Seo, O.J. Kwon, C.H. Park, and H.J. Hwang, *RSC Adv.* 4, 43811 (2014).
11. S. Chen, K.F. Cai, F.Y. Li, and S.Z. Shen, *J. Electron. Mater.* 43, 1962 (2014).
12. J. Li, Q. Tan, J.F. Li, D.W. Liu, F. Li, Z.Y. Li, M. Zou, and K. Wang, *Adv. Funct. Mater.* 23, 4317 (2013).
13. X.A. Fan, J.Y. Yang, R.G. Chen, H.S. Yun, W. Zhu, S.Q. Bao, and X.K. Duan, *J. Phys. D Appl. Phys.* 39, 740 (2006).
14. J.J. Shen, L.P. Hu, T.J. Zhu, and X.B. Zhao, *Appl. Phys. Lett.* 99, 124102 (2011).
15. S. Wang, H. Li, R. Lu, G. Zheng, and X. Tang, *Nanotechnology* 24, 285702 (2013).
16. T.E. Svechnikova, P.P. Konstantinov, and G.T. Alekseeva, *Inorg. Mater.* 36, 677 (2000).
17. S. Wang, J. Yang, T. Toll, J. Yang, W. Zhang, and X. Tang, *Sci. Rep.* 5, 10136 (2015).
18. W. Liu, X. Yan, G. Chen, and Z. Ren, *Nano Energy* 1, 42 (2012).
19. L.D. Zhao, S.H. Lo, J. He, H. Li, K. Biswas, J. Androulakis, C.I. Wu, T.P. Hogan, D.Y. Chung, V.P. Dravid, and M.G. Kanatzidis, *J. Am. Chem. Soc.* 133, 20476 (2011).
20. S. Wang, X. Tan, G. Tan, X. She, W. Liu, H. Li, H. Liu, and X. Tang, *J. Mater. Chem.* 22, 13977 (2012).
21. S. Hwang, S.I. Kim, K. Ahn, J.W. Roh, D.J. Yang, S.M. Lee, and K.H. Lee, *J. Electron. Mater.* 42, 1141 (2013).
22. I.H. Kim, S.M. Choi, W.S. Seo, and D.I. Cheong, *Nanoscale Res. Lett.* 7, 2 (2012).
23. K.H. Lee, H.S. Kim, S.I. Kim, E.S. Lee, S.M. Lee, J.S. Rhyee, J.Y. Jung, I.H. Kim, Y. Wang, and K. Koumoto, *J. Electron. Mater.* 41, 1165 (2012).
24. D. Jung, K. Kurosaki, S. Seino, M. Ishimaru, K. Sato, Y. Ohishi, H. Muta, and S. Yamanaka, *Phys. Status Solidi B* 251, 162 (2014).
25. G. Tan, F. Shi, S. Hao, H. Chi, L.D. Zhao, C. Uher, C. Wolverton, V.P. Dravid, and M.G. Kanatzidis, *J. Am. Chem. Soc.* 137, 5100 (2015).
26. G. Tan, L.D. Zhao, F. Shi, J.W. Doak, S.H. Lo, H. Sun, C. Wolverton, V.P. Dravid, C. Uher, and M.G. Kanatzidis, *J. Am. Chem. Soc.* 136, 7006 (2014).